ACS Catalysis

Research Article

pubs.acs.org/acscatalysis

Development of NiCu Catalysts for Aqueous-Phase Hydrodeoxygenation

Jacob G. Dickinson and Phillip E. Savage*

Department of Chemical Engineering, University of Michigan, Ann Arbor, Michigan 48109, United States

Supporting Information

ABSTRACT: Herein, we report on the development of supported Ni and Raney Ni catalysts doped with Cu for the hydrothermal hydrodeoxygenation (HDO) of *o*-cresol. Raney Ni catalysts doped with >10 wt % Cu show a significant reduction in gasification activity and produce a higher yield of liquid products than the unmodified Raney Ni catalyst. Adding Cu did not, however, increase the yield of the desired HDO products, liquid hydrocarbons. The addition of acid sites to the catalysts, by supporting Ni and NiCu on Al_2O_3 and by calcining the Raney Ni to produce Al_2O_3 within the catalyst, however, did significantly increase the HDO activity of the catalysts such that yields of liquid hydrocarbons exceeded 60%. Two catalysts, a novel calcined 5% Raney NiCu catalyst and a $NiCu/Al_2O_3$ catalyst, produced the highest liquid hydrocarbon yields to date (~70%) for stable, non-noble metal, hydrothermal HDO catalysts.

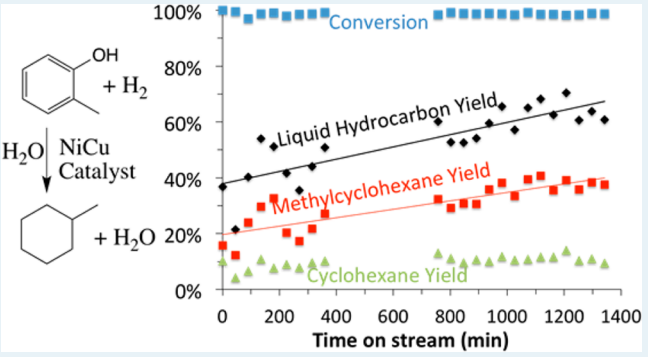

KEYWORDS: *hydrodeoxygenation, hydrothermal, Raney Ni, o-cresol, aqueous phase, NiCu catalysts, alumina, biomass*

1. INTRODUCTION

Hydrodeoxygenation (HDO) is an enabling technology for the conversion of biomass into liquid fuels and chemicals because it decreases the viscosity and increases the energy density of bio-oils. HDO has been the focus of several extensive reviews.[1−3] The present work focuses on HDO occurring in a high-temperature, aqueous (i.e., hydrothermal) reaction environment. Hydrothermal HDO is of interest for several reasons: First, most biomass liquefaction technologies (e.g., fast pyrolysis, pyrolysis, hydrothermal liquefaction) result in a mixture or solution of bio-oil and water that can range from 20 to 30 wt % water for bio-oils obtained from the fast pyrolysis of lignocellulosic biomass[4] and to 80−90 wt % water for the reactor effluent from the hydrothermal liquefaction (HTL) of microalgae.[5] The water content in the reactor effluent is a function of the type of biomass, the water content of the biomass, and the processing conditions. Separation of the bio-oil and water after the biomass treatment step is sometimes possible, but it can be difficult when the material is a single phase or an oil/water emulsion.[6] Second, the oxygen content of bio-oil ranges from 5 wt % for bio-oils obtained from the HTL of microalgae[5,7] to 50 wt % for bio-oils obtained from the fast pyrolysis of lignocellulosic biomass.[4] When this oxygen is removed from the bio-oil with H_2, water is formed. Stoichiometry indicates that a bio-oil with 15 wt % oxygen will form an oxygen-free bio-oil and water mixture containing 17 wt % water upon complete HDO. Therefore, water will be present, likely in high quantities, during HDO.

Hydrothermal HDO presents significant challenges to catalyst stability and activity. Many common hydrotreating catalysts, such as NiMo and CoMo, oxidize under hydrothermal conditions,[8] and common catalyst supports, such as γ-Al_2O_3 and SiO_2, may be unstable under some hydrothermal conditions.[8−10] This realization has led most researchers to use noble metal catalysts (Pt, Pd, Ru, and Rh) for hydrothermal HDO.[11] Dumesic and co-workers have pioneered the conversion of sugars and biofuel byproduct molecules, such as ethylene glycol, to H_2 and alkanes.[12−16] Many of these studies have focused on aqueous-phase reforming of sugars with the goal of producing H_2, but the authors found that some metals, such as Ni, Rh, and Ru, were more selective for alkane production than for gas formation.[14] Huber et al. examined the conversion of sorbitol over Pt and achieved a high gas phase hydrocarbon yield and found the catalyst to be stable over a six-day period.[15] Furthermore, they found that the liquid alkane yield was greater when they used a mixture of Pt/Al_2O_3 and SiO_2−Al_2O_3. This increase in liquid alkane yield was attributed to the presence of the solid acid (SiO_2−Al_2O_3) catalyst.

Lercher and co-workers have extensively examined the HDO of phenolic molecules between 150 and 200 °C using Pd/C with H_3PO_4 or HZSM-5[17−19] and achieved complete conversion and high selectivity (>80%) to cycloalkanes. Interestingly, without the acid catalyst (i.e., H_3PO_4 or HZSM-

Received: April 25, 2014
Revised: June 23, 2014
Published: June 27, 2014

5), no cycloalkanes were observed. In later studies, they combined the active metal, Pd, and acid catalysts into a single, bifuntional catalyst, Pd/HBEA, that produced primarily larger, oxygen-free hydroalkylation products from phenolic molecules.[20]

Savage and co-workers have also made significant progress in catalytically converting bio-oils and bioderived molecules into liquid hydrocarbons under hydrothermal conditions.[21−30] In general, these studies have taken place at higher temperatures (350−500 °C) and pressures (150−305 bar) than those examined by Dumesic and Lercher (∼200 °C, ∼25 bar). These studies revealed that Pt/C is an active and stable catalyst for the decarboxylation of palmitic acid and the hydrothermal HDO of *o*-cresol and benzofuran.[21,22,29] It is important to note that unlike the work of Lercher et al., these reactions did not require an additional acid catalyst to perform HDO. Nonetheless, these studies have focused on using noble metal catalysts whose high cost make them undesirable.

Reports of active non-noble metal catalysts for hydrothermal HDO are rare. Lercher and associates examined the use of Raney Ni with homogeneous (H_3PO_4 and acetic acid) or solid acid catalysts (Nafion/SiO_2) and determined that only the Raney Ni and Nafion/SiO_2 catalyst combination was effective at producing cycloalkanes from 4-*n*-propylphenol at 200 °C.[31] Again, the researchers determined that the solid acid catalyst was essential for producing cycloalkanes, as conversions and selectivities were negligible without it. These researchers have also examined the use of Ni/HZSM-5 and Ni/γ-Al_2O_3−HZSM-5 catalysts for phenol and phenolic monomer hydrothermal HDO and obtained a 100% yield of hydrocarbons between 200 and 250 °C.[32,33] Unfortunately, though, these catalysts showed substantial deactivation in catalyst recycle experiments, even with catalyst regeneration occurring between cycles, because of catalyst particle sintering, Ni leaching, and structural changes to the catalyst support.[32]

To address this need to develop active and stable non-noble metal catalysts for hydrothermal HDO, we previously examined a Raney Ni catalyst doped with 10 wt % Cu and found the catalyst to be active, selective, and stable for hydrothermal HDO at 380 °C.[21] Cu was chosen as a dopant because the base Raney Ni catalyst was active for C−C bond hydrogenolysis, producing primarily methane from the *o*-cresol fed to the reactor, and because Elliot et al. showed that Cu was inactive for gasification.[8] We associated this increase in selectivity to liquid phase products to the fact that, in a different catalyst system, Cu reduces the adsorption energy of aromatic molecules when alloyed with Pd to make a PdCu catalyst.[34] The present study expands on this previous work to examine the effect of Cu content on the products, selectivities, and yields from reacting *o*-cresol, a model oxygen-containing compound found in most bio-oils,[35,36] with H_2 over various catalysts. This work shows that increasing Cu content drastically reduces the gasification activity of the Raney NiCu catalysts but is ineffective at increasing the yield of the desired liquid hydrocarbons. To increase the liquid hydrocarbon yield, we added Al_2O_3 to the catalysts through two parallel approaches. One approach was to synthesize a NiCu/Al_2O_3 catalyst, and the second was to calcine the Raney Ni catalyst, thereby oxidizing the Al in the Raney Ni catalyst to Al_2O_3. With these catalyst modifications, we provide, to the best of our knowledge, the first report of a high (≥60%) and stable liquid hydrocarbon yield by using only a non-noble metal catalyst for HDO in hydrothermal conditions.

2. MATERIALS AND METHODS

This section provides the details of the materials and methods used to complete the experimental work and analyses.

2.1. Materials. We procured all solvents, reagents, and catalyst precursors from Fischer Scientific (≥99% purity) and used them as received. Raney Ni 2800 was obtained from Sigma-Aldrich, and the γ-AlOOH that was used as a catalyst support and a catalyst bed diluent was obtained from Morton Thiokol. γ-AlOOH was converted to γ-Al_2O_3 during the calcination and reduction of the catalysts (shown later); therefore, we refer to all such catalysts as Al_2O_3-supported. The ZrO_2 was obtained from Alpha Aesar, and deionized water was prepared in house.

2.2. Catalyst Synthesis. We synthesized the Raney NiCu catalysts by dissolving $Cu(NO_3)_2{\cdot}2.5H_2O$ in 5 mL of ethanol, adding this solution to reduced Raney Ni, heating the resulting mixture to 100 °C in a sealed vial for 1 h, and then reducing the catalyst in flowing H_2 at 400 °C for 3 h with a 5 °C/min ramp rate. For example, to synthesize the 5% Raney NiCu catalyst, we added, by puncturing the parafilm covering the vial, a solution containing 0.137 g of $Cu(NO_3)_2{\cdot}2.5H_2O$ and 5 mL of ethanol to an Ar-filled vial containing 0.713 g of reduced Raney Ni before carrying out the heating and reduction procedures above.

The Al_2O_3- and ZrO_2-supported catalysts were synthesized by impregnating the support with a $Ni(NO_3)_2{\cdot}6H_2O$ or a $Ni(NO_3)_2{\cdot}6H_2O$ and $Cu(NO_3)_2{\cdot}2.5H_2O$ solution in DI H_2O. In general, to achieve the desired metal loadings, we performed two impregnations of the γ-AlOOH for the Al_2O_3-supported catalysts, and three impregnations of the ZrO_2 for the ZrO_2-supported catalyst. For example, to synthesize the 10% 0.5% NiCu/Al_2O_3 catalyst, we performed two impregnations of 4.5 g of γ-AlOOH with a solution that contained 6.6 g of $Ni(NO_3)_2{\cdot}6H_2O$ and 0.25 g of $Cu(NO_3)_2{\cdot}2.5H_2O$ in 13.2 mL of DI H_2O. Following each impregnation, we dried the catalysts at 110 °C for 12 h and then calcined them by increasing the temperature at 10 °C/min to 400 °C, where the temperature was held for 4 h. The calcined catalysts were crushed and sieved (150 μm) and then reduced in flowing H_2 by increasing the temperature at 5 °C/min to 400 °C, where the temperature was held for 3 h.

Last, to produce the calcined Raney Ni and calcined Raney NiCu catalysts, we heated the Raney Ni in DI water at 80 °C for 3 h, followed by drying and calcining the catalysts using the procedure outlined above. The calcined 5% Raney NiCu catalyst was synthesized by adding 0.590 g of $Cu(NO_3)_2{\cdot}2.5H_2O$ in 5 mL of ethanol to 3.047 g of calcined Raney Ni. The resulting mixture was heated and reduced using the procedure discussed for producing the Raney NiCu catalysts.

2.3. Catalyst Characterization. We performed X-ray Diffraction (XRD), transmission electron microscopy (TEM), and CO temperature-programmed desorption (TPD) using catalysts passivated overnight at 70 °C in 1% O_2 in He. XRD characterization was performed on a Rigaku Miniflex 600, TEM/STEM was performed on a Jeol 2010f, and CO TPD was performed on a Micromeritics Autochem 2910. The passivated catalysts were reduced in situ at 430 °C for 180 min, prior to the TPD experiments. CO was added to the catalyst surface at 25 °C, and the catalyst was heated at 10 °C/min to 550 °C.

2.4. Batch Reactor Procedure. For each hydrothermal HDO experiment, the reduced catalysts were transferred to an Ar glovebox in the reduction tube to minimize oxygen exposure. The reduced catalysts were loaded into 4.1 mL

dx.doi.org/10.1021/cs500562u | ACS Catal. 2014, 4, 2605−2615

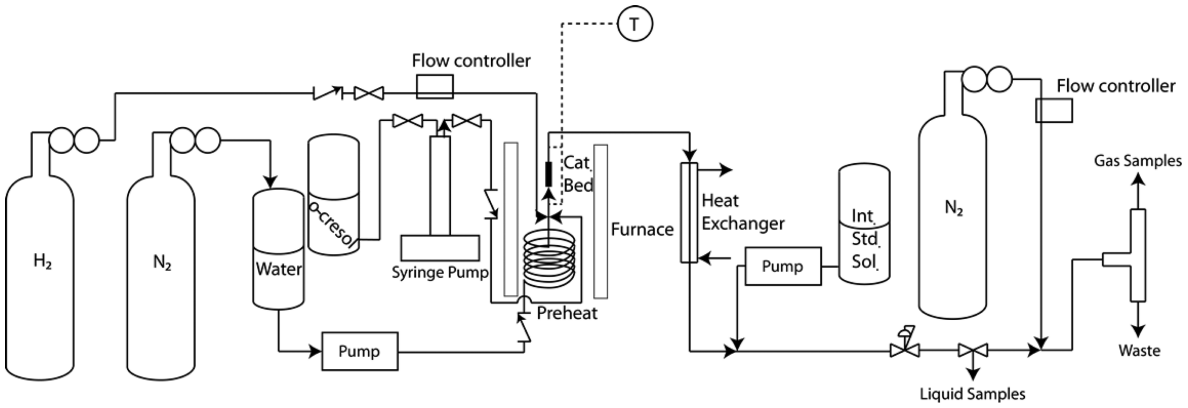

Figure 1. Flow reactor process flow diagram.

Swagelok batch reactors in the Ar glovebox, and the open end of each reactor was sealed with parafilm. The batch reactors were filled outside of the glovebox with 0.67 mL of DI H_2O and either 20 or 100 mg of *o*-cresol by poking holes through the parafilm, thereby minimizing exposure of the catalyst to air. The batch reactors were then capped, purged with He, and pressurized with He and H_2. Details on the construction, pressurization, extraction, gas analysis, and liquid product analysis are available in our previous work.[22] In short, we heated the reactors to 380 °C in a fluidized sand bath, quenched the reactors in water, analyzed the gas content of the reactors with GC/TCD, extracted the reactors with 10 mL of acetone, and analyzed the liquid contents of the reactors with GC/FID. In some instances, multiple reactions were run at a single reaction condition to obtain estimates of the experimental uncertainty, represented by one standard deviation. We report data only from reactors with carbon balances >80%, but in general, the carbon balances were >90%.

2.5. Flow Reactor Description. We used two different flow reactor configurations. The first configuration used a sandbath as the heating source and had a feed that contained DI water, formic acid, and *o*-cresol. This flow reactor configuration was detailed in our previous work[21] and in the present work was used only with the 2% Raney NiCu catalyst. A second flow reactor configuration, shown in Figure 1, is similar to the previous setup, but with a few major improvements. First, H_2 was delivered to the flow reactor with a mass flow controller, instead of using the in situ decomposition of formic acid as the H_2 source. Second, separate pumps for DI water and *o*-cresol allowed for varying concentrations of *o*-cresol to be fed to the reactor. Last, we used a tube furnace as the heating source of the reactor to allow for faster heat up and cool down times.

The modified flow reactor, shown in Figure 1, has three 316 stainless steel inlet lines. Chrom Tech Series III pumps fed DI water and the internal standard solution to the reactor and cooled reactor effluent, respectively. *o*-Cresol, heated to 35 to 40 °C by heat tape, was fed by an ISCO 260D syringe pump, and H_2 was fed through a Brooks 5850 TR mass flow controller from a 6000 psig H_2 cylinder. The preheating tubing within the Applied Test Systems furnace, which was controlled by an Omega PID controller, was 1/16 in. o.d. tubing. The water, H_2, and *o*-cresol preheating lines were 80, 60, and 15 in. in length, respectively, and mixed in a cross fitting prior to entering the catalyst bed. The temperature within this cross fitting was monitored by a thermocouple and data logger. The 3.5 in. catalyst bed was constructed from 1/4 in. o.d. tubing with 5 μm Hastelloy frits placed at both ends. The catalyst bed was loaded with catalyst and γ-AlOOH, a diluent, in the Ar glovebox. We covered the ends of the catalyst bed with parafilm in the glovebox to minimize the exposure of the catalyst to air when the catalyst bed was transferred to the flow reactor. A second thermocouple, positioned in a T fitting, measured the temperature of the product stream exiting the catalyst bed. A tube-in-tube heat exchanger cooled the reactor effluent to room temperature, and a backpressure regulator maintained the desired reaction pressure.

We added an internal standard solution consisting of 4-isopropylphenol (4 g/L) in 2-propanol to the cooled reactor effluent prior the backpressure regulator to form a single liquid phase and to provide an internal standard for use in product quantification. N_2 was added (15−20 mL/min) to the reaction stream through an Omega 5400/5500 mass flow controller after the backpressure regulator to provide a reference gas. A Gilson 223 fraction collector with an automated switching valve collected liquid samples in test tubes containing ∼3 mL of 2-propanol. When the fraction collector was not collecting liquid samples, the reactor effluent was diverted to a 250 mL flash column that separated the liquid and gas products. The liquid products were sent to a waste container while the gas products were sent to the GC/TCD. The liquid samples were analyzed on an Agilent 6890N gas chromatograph with a flame ionization detector using a 50m HP-5MS capillary column. The injected sample, 1 μL, was heated by an inlet at 310 °C and separated by the capillary column by holding the column at 35 °C for 10 min and then ramping the oven temperature at 2 °C/min to 50 °C, 10 °C/min to 160 °C, 30 °C/min to 300 °C, and holding for 2 min. An Agilent 6890N gas chromatograph with a mass spectrometric detector used this same method and column to determine the identities of some molecules.

2.6. Flow Reactor Procedure. To start up the flow reactor shown in Figure 1, we first attached the catalyst bed to the reactor, then pressurized the system with 70 bar H_2 to check for leaks. After confirming the absence of leaks, we released the reactor pressure and began flowing H_2 at 50−100 mL/min while heating the reactor to 550 °C for at least 1 h for the in situ catalyst reduction. We then cooled the reactor to ∼400 °C and started flowing water, H_2, and *o*-cresol. For the calcined Raney Ni and calcined 5% Raney NiCu catalysts, we set the H_2O, *o*-cresol, and H_2 flow rates to 1 mL/min, 0.030 mL/min, and 0.006 mol/min, respectively, to build the reaction pressure. Upon the reactor's reaching ∼240 bar, we lowered the H_2O

dx.doi.org/10.1021/cs500562u | ACS Catal. 2014, 4, 2605−2615

flow rate to the desired steady state value of 0.270 mL/min, while maintaining the other flow rates. At this point, we also started the internal standard solution flowing at 0.400 mL/min and the N_2 reference gas flowing at 20 mL/min. The startup procedure for the 10%, 0.5% $NiCu/Al_2O_3$ catalyst differed only in the H_2O flow rate, which was set at 0.270 mL/min during the entire startup period. Upon reaching the desired temperature of 365 °C at the mixing point thermocouple and the desired reactor pressure of 280 bar, we began collecting samples. We found that the reactor took approximately 225 min to achieve steady carbon balances, and we report this time as 0 min on-stream.

2.7. Data Analysis. We calculated conversion, yield, selectivity, and carbon recovery as follows:

$$\text{conversion} = 1 - \frac{C_{oc,e}}{C_{oc,O}} \quad (1)$$

$$\text{yield} = \frac{C_i}{C_{oc,O}} \quad (2)$$

$$\text{selectivity} = \frac{C_i}{\sum C_i} \quad (3)$$

$$\text{carbon recovery} = \frac{\sum C_i}{C_{oc,O}} \quad (4)$$

where $C_{oc,e}$, $C_{oc,o}$, and C_i refer to the concentrations, in mol C/L, of *o*-cresol exiting the reactor, of *o*-cresol entering the reactor, and of any product, respectively. We also will refer to the liquid hydrocarbon yield, which is the sum of the yields of all hydrocarbons in the liquid phase reactor effluent. On occasion, the flow reactor would release a large volume of gas, resulting in a slight pressure drop in the reactor. This increased gas flow resulted in high yields of the carbon-containing gases (i.e., methane and CO_2) and high carbon recoveries (≥120%) if sampling occurred simultaneously with a gas release. When such anomalous data were collected, we removed them from the data set.

3. RESULTS AND DISCUSSION

This section is divided into two major parts. The first section examines the effect of Cu loading on product yields and selectivities for the hydrothermal HDO of *o*-cresol. The second section discusses improvements to the NiCu catalysts made through the addition of acid sites. Within each major section, we first discuss reaction results and then examine the findings of the catalyst characterization.

3.1. Raney NiCu Catalysts and the Effect of Cu Loading. Previous work[21] indicates that Raney Ni 2800 promoted with 10 wt % Cu is an active and stable catalyst for hydrothermal HDO. The goal of this section is to examine the effect of Cu loading and to develop a catalyst and reaction scheme for hydrothermal HDO that produces high liquid hydrocarbon yield. To achieve this goal, the catalyst must not only be active, it must also be selective for C−O bond hydrogenolysis.

3.1.1. 2% Raney NiCu. Previous work[21] showed that a 10% Raney NiCu catalyst had a lower HDO turnover frequency (TOF) than did unmodified Raney Ni. Further, the total activity (i.e., TOF for conversion) of the 10% Raney NiCu catalyst is even more suppressed when compared with the unmodified Raney Ni catalyst. We desired to learn whether reducing the Cu content would improve overall and HDO activity without diminishing the selectivity increases and, therefore, the higher liquid hydrocarbon yield observed with the 10% Raney NiCu catalyst. Therefore, we synthesized a 2% Raney NiCu catalyst and tested this catalyst in the flow system described previously[21] at 380 °C using formic acid decomposition as the H_2 source.

Figure 2 shows the variation of conversion and liquid hydrocarbon yield with time on-stream (TOS). The most

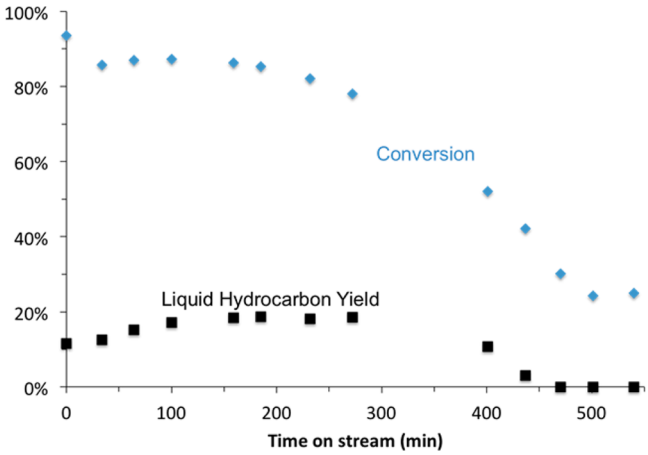

Figure 2. Conversion and liquid hydrocarbon yield from reacting *o*-cresol over 2% Raney NiCu. W/F = 56 min; 380 °C; 305 bar; feed solution (ambient conditions): 24.7 g/L *o*-cresol, 147 mL/L formic acid, balance DI H_2O; feed flow rate (ambient temperature) = 0.218 mL/min; 430 °C in situ H_2 catalyst reduction.

abundant liquid hydrocarbon products were toluene, methylcyclohexane, benzene, and cyclohexane. In addition to these products, oxygenated products consisting primarily of methylcyclohexanone and phenol formed. Methane and CO_2 were the only gaseous products, but because of the presence of formic acid in the reactor feed, it is unclear whether these carbon-containing molecules originate from the formic acid or *o*-cresol.

Figure 2 shows that the maximum liquid hydrocarbon yield of 19% occurred around 200 min on stream. This maximum liquid hydrocarbon yield is similar to the 21 ± 4% average liquid hydrocarbon yield obtained previously from a 10% Raney NiCu catalyst using the same reaction conditions.[21] After reaching this maximum, the liquid hydrocarbon yield quickly declined to 0% at 470 min on-stream and thereafter. Likewise, conversion decreased rapidly after 200 min on-stream. It is clear that the 2% Raney NiCu catalyst deactivates rapidly after ∼240 min on-stream.

The cause of the deactivation is unknown and is beyond the primary focus of this work. We did perform several simple experiments, however, that permit speculation regarding the cause of deactivation. We previously reported that CO is in the reaction stream that contacts the catalyst bed. Figure 3 shows the results from CO TPD of the unmodified Raney Ni catalyst and the 10% Raney NiCu catalyst used previously.[21] These results will be discussed more thoroughly in a later section. At present, we will simply remark that CO remained adsorbed to both the Raney Ni and 10% Raney NiCu catalysts at temperatures approaching 600 °C. This finding is important because it points to a possible cause of catalyst deactivation—CO poisoning—and a possible means of regenerating the catalyst: reduction of the catalyst at high temperature (e.g., 550

dx.doi.org/10.1021/cs500562u | ACS Catal. 2014, 4, 2605−2615

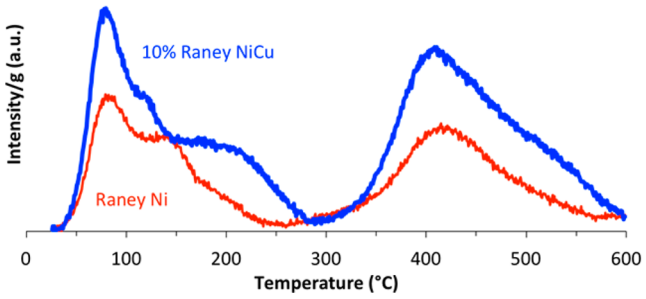

Figure 3. CO temperature-programmed desorption spectra of Raney Ni and 10% Raney NiCu.

°C) in flowing H_2. Literature also indicates that CO_2, when reacted over a Ni catalyst, can form adsorbed CO.[37] The preferential pathway for the removal of adsorbed CO when H_2 is present is through a HCO or COH pathway that converts bound CO to methane.[38]

Figure 4 shows the liquid hydrocarbon yield from three cycles of reacting *o*-cresol over the same 2% Raney NiCu

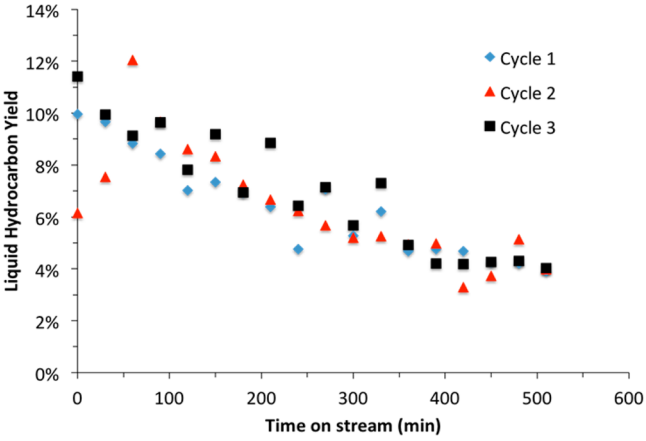

Figure 4. Liquid hydrocarbon yield from reacting *o*-cresol over 2% Raney NiCu. W/F = 80 min; 380 °C; 305 bar; feed solution (ambient conditions): 24.7 g/L *o*-cresol, 147 mL/L formic acid, balance DI H_2O; feed flow rate (ambient temperature) = 0.200 mL/min; 550 °C in situ H_2 catalyst reduction between runs.

catalyst that was used in Figure 2 (Table S1, Supporting Information). Each cycle consisted of reducing the catalyst at 550 °C in flowing H_2, then passing the feed solution over the catalyst for 720 min. It is clear from Figure 4 that the liquid hydrocarbon yields for each cycle overlap, indicating that the HDO activity of the catalyst was regenerated after each cycle by simply rereducing the catalyst. This result is consistent with CO poisoning, causing the loss in catalyst activity, but it does not preclude other methods of deactivation. The catalyst could be losing activity from oxidation of the Ni metal by supercritical water or from some other unknown catalyst poison. Other common deactivation causes, such as sintering or coking, are unlikely because these conditions are irreversible by reduction.

3.1.2. Cu Loading Effects. This section elucidates the effect of Cu loading on the HDO selectivity of 1−40 wt % Raney NiCu catalysts using H_2 (rather than formic acid) as the reductant to avoid the formation of CO. We performed these reactions in 4.1 mL batch minireactors to rapidly screen these catalysts.

Figure 5 and Supporting Information (SI) Table S2 shows that at low Cu loading (e.g., 1−7%), the conversion of *o*-cresol

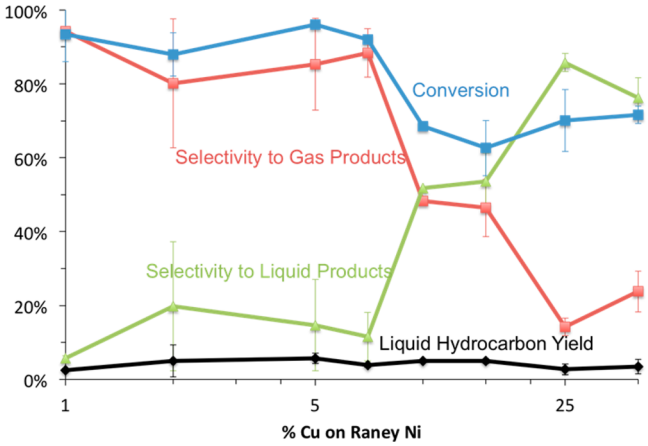

Figure 5. Effect of Cu loading for Raney NiCu catalysts on selectivity, conversion, and liquid hydrocarbon yield in 4.1 mL reactors. Conditions: 380 °C, 30 min, 20 mg catalyst, 20 mg of *o*-cresol, 0.67 mL DI H_2O, 19 bar H_2 (STP), $w \times t/m$ = 30 min, 17:1 H_2 to *o*-cresol.

was nearly 100%, and the selectivity to gas products, such as methane (55−68% yield), ethane (~1% yield), and CO_2 (15−30% yield), was high. Selectivity to liquid products was low. The liquid products were mainly oxygenated intermediates, such as phenol (1.4−8.3% yield), cyclohexanone (0−2.7% yield), methylcyclohexanone (0.4−2.4% yield), and methylcyclohexanol (0−2.4% yield).

There was a dramatic shift in product selectivities and conversion when the Cu content of the Raney NiCu catalyst increased beyond 7% Cu. Figure 5 shows that the conversion of *o*-cresol drops beyond 7% Cu loading and remains relatively steady at ~70%. In addition, between 7 and 25% Cu, the product selectivities shift from forming gas to forming liquid products. Again, methane and CO_2 were the main gases whereas the aforementioned oxygenated intermediate molecules were present in high yields (SI Table S2).

These results support the conclusion that Cu decreases the hydrocracking (C−C bond hydrogenolysis with H_2) activity of the catalyst. It is likely, on the low-Cu-loaded catalysts, that cyclohexanol, after forming from the hydrogenation of cyclohexanone, continues to react to form methane. This hypothesis is supported by literature showing that Ni is a more active hydrogenation and hydrocracking metal than Cu.[8] The lower overall activity of the high-Cu-loaded catalysts manifests in the decreased conversion observed. In contrast to the conversion and liquid and gas product selectivities in Figure 5, the liquid hydrocarbon yield varied little as the Cu content of the catalysts was varied. The liquid hydrocarbon yield varied only from a low of 2.5 ± 0.2% for the 1% Raney NiCu catalyst to 5.6 ± 1.4% for the 5% Raney NiCu catalyst.

The goal of this work was to produce a non-noble metal catalyst that is active, selective, and stable for hydrothermal HDO because such a catalyst would result in high liquid hydrocarbon yield while minimizing the formation of lower-value gas products. The results above indicate that Cu doping the Raney Ni catalyst is itself insufficient to achieve this goal because the addition of Cu results only in minimizing unwanted gas products and not in increasing the yield of the desired liquid hydrocarbon products.

dx.doi.org/10.1021/cs500562u | *ACS Catal.* 2014, 4, 2605−2615

3.1.3. Raney NiCu Catalyst Characterization. The reaction results presented in section 3.1.2 indicate that the addition of Cu to a Raney Ni catalyst has a dramatic effect on the product selectivities when *o*-cresol is reacted at 380 °C in supercritical water. This section elucidates the morphology of the Raney NiCu catalysts by discussing the results from titration, diffraction, and microscopy experiments used to characterize the catalysts.

Figure 3 shows the results of CO TPD of both the unmodified Raney Ni and 10% Raney NiCu catalysts. Both spectra contain two major peaks at 75 and 405 °C. The Raney Ni spectrum contains one shoulder between 105 and 140 °C, whereas the Raney NiCu spectrum contains two shoulders: one between 105 and 115 °C and the other, broader shoulder, between 145 and 210 °C. This second broad shoulder is an entirely new feature in the 10% Raney NiCu spectrum that was not observed in the Raney Ni spectrum. Both spectra were integrated, and the 10% Raney NiCu catalyst adsorbed 1.7 times the CO of the Raney Ni catalyst. The new shoulder and the increased CO uptake suggest that a new phase is formed when the Raney Ni catalyst is doped with Cu, but the results do not provide direct evidence of the type of phase the Cu forms. We also examined a Cu standard (100 nm Cu particles) under the same reduction and TPD conditions and found no significant CO uptake because the Cu particles sintered. Therefore, it is likely that the Cu and Ni in the 10% Raney NiCu catalyst form an alloy as a result of the relatively high CO uptake observed.

Figure 6 shows the XRD patterns of the 1−40% Raney NiCu catalysts. The dominant features of each diffraction pattern at

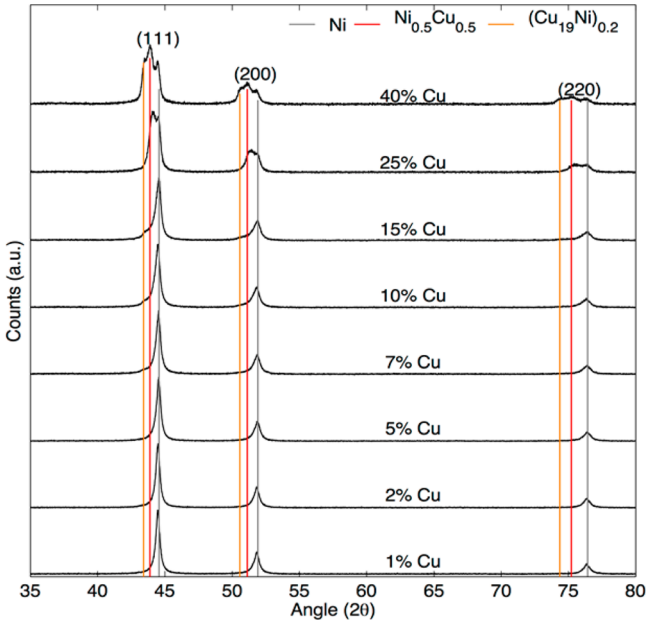

Figure 6. X-ray diffraction patterns of the Raney NiCu catalysts. Conditions: passivated in 1% O_2 at 70 °C overnight, Cu Kα source, 40 kV, 15 mA, 1.25°/min.

low Cu loading (1−7%) are the Ni planes. As the Cu loading increases, a peak forms at the base of the Ni(111) peak in the 10% Raney NiCu catalyst. Further increases in Cu loading increase the size of this peak, identified as a $Ni_{0.5}Cu_{0.5}$, indicating the formation of an alloy of Ni and Cu. The 40% Raney NiCu catalyst shows the formation of a third peak in the (111) plane, identified as a Cu-rich phase, $(Cu_{19}Ni)_{0.2}$. In addition to the (111) plane, one also observes the formation of the $Ni_{0.5}Cu_{0.5}$ and $(Cu_{19}Ni)_{0.2}$ phases in the (200) and (220) planes. These results indicate that Ni and Cu form an alloy under the synthesis and reduction conditions used and that at low to moderate Cu loading, this alloy appears to be roughly equal parts Ni and Cu.

Figure 7 shows TEM and STEM images of the 10% Raney NiCu catalyst. Figure 7a shows a TEM image of the catalyst

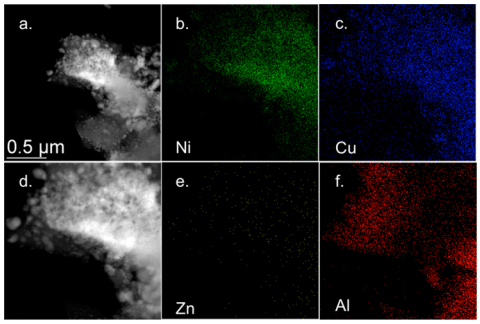

Figure 7. TEM and STEM elemental maps of 10% Raney NiCu. (a) The original TEM image of the catalyst. (d) The STEM image taken of the section of the catalyst used for the elemental map. (b, c, e, f) The result from elemental maps of Ni, Cu, Zn, and Al, respectively.

particle examined. Figure 7d shows the STEM image used to generate the elemental map. We calculated the *x* distance across Figure 7d, using the scale bar from Figure 7a and common points in both images, as 870 nm. Figure 7b,c,e,f shows the elemental maps of Ni, Cu, Zn, and Al. One expects Ni, Cu, and Al to be present in the catalyst. Zn, on the other hand (Figure 7e), served as a control element to determine the amount of background signal one should expect. Examination of Figure 7e indicates that the background signal is low compared with the signals obtained from the other elements. Figure 7f shows that the Al appears to be segregated to both ends of the catalyst particle examined, with relatively little Al present in the middle of the image. This segregation is likely a result of the leaching methods that are used to remove Al from the Ni matrix during the synthesis of Raney Ni.

Figure 7b,c indicates that Ni and Cu appear to spread evenly across the catalyst surface. This finding likely indicates that the Cu added to the catalyst is not present in Cu islands but, rather, is present in a NiCu alloy that is relatively evenly dispersed on the catalyst surface. This finding is also in agreement with the XRD and TPD results presented earlier. All of the catalyst characterization findings are consistent with the results of Huber and Shabacker, who used a Sn-doped Raney Ni catalyst for aqueous phase reforming reactions and found that the Sn incorporated in the Ni catalyst.[39−41]

3.2. Improved Ni-Based Hydrothermal HDO Catalysts with the Addition of Acid Sites. Section 3.1 showed that the addition of Cu to Ni catalysts suppresses gasification activity, but has little effect on the HDO activity of these catalysts. In short, the Raney NiCu catalysts are active for the hydrogenation of *o*-cresol but are not sufficiently active for the C−O hydrogenolysis required for HDO. Recent research suggests that acid sites are essential for hydrothermal HDO reactions over Ni catalysts.[31,42] Zhao et al. found that the Raney Ni 4200 and 2400 are active for HDO only when an additional acid catalyst (in this case, Nafion supported on SiO_2) was added to

dx.doi.org/10.1021/cs500562u | *ACS Catal.* 2014, 4, 2605−2615

the reaction mixture.[31] Mortensen et al. found that the nonhydrothermal HDO of phenol occurred more rapidly on acidic supports, such as ZrO_2 and Al_2O_3, leading these researchers to speculate that the HDO reaction actually occurred at the metal/support interface.[42]

This section elucidates the influence of added acidity on the product yields and selectivities by modifying the reaction system in three ways. First, we used the 10% Raney NiCu catalyst in an aqueous solution of HCl or H_2SO_4. Second, we synthesized Ni and NiCu catalysts on acidic supports (e.g., Al_2O_3 and ZrO_2). Third, we further modified the Raney Ni catalyst by oxidizing some of the Al in the catalyst to Al_2O_3 by calcining the catalyst in air at 400 °C (see section 2). This calcined Raney Ni catalyst is a novel catalyst that, to the best of our knowledge, has never before been used for HDO. The only prior report we found of intentionally producing Al_2O_3 through calcination on a Raney Ni catalyst used the Al_2O_3 as a binder for an extruded catalyst.[43]

3.2.1. Batch Experiments with Acidic Ni Catalysts. We examined a variety of catalysts in 4.1 mL batch minireactors to quickly assess their activity for hydrothermal HDO under a variety of conditions. Table 1 summarizes these results and

Table 1. Summary of Catalysts Tested in 4.1 mL Batch Reactors[a]

catalyst	X, %	LH yield, %	S_{liq}, %	time (min)	$W \times t/m$ (min)
10% Raney NiCu	37−80	0−7	65−87	15−45	1.5−4.5
10% Raney NiCu + HCl[b]	1−4	0		15−60	1.5−6.0
10% Raney NiCu + H_2SO_4[c]	0−5	0−1		30−60	3.0−6.0
10% Ni/Al_2O_3	54−93	12−35	85−91	30−150	0.15−1.5
10% Ni/ZrO_2	14−67	0−8	64−98	15−180	0.3−1.8
calcined Raney Ni	57−88	3−12	44−68	15−60	1.5−6.0

[a]Conditions: 380 °C, 15−180 min, 10 mg of catalyst, 100 mg of *o*-cresol, 0.67 mL of DI H_2O or DI water acid solution, 41 bar H_2 (STP), 6:1 H_2 to *o*-cresol, X = conversion, LH = liquid hydrocarbon, S_{liq} = selectivity to liquid products. [b]1.04 wt % HCl in DI water. [c]0.2 wt % H_2SO_4 in DI water

conditions used. These experiments used less catalyst (10 vs 20 mg), more *o*-cresol (100 vs 20 mg), and a lower H_2-to-*o*-cresol molar ratio (6:1 vs 17:1) than did the batch reactions that generated Figure 5. These reaction conditions were chosen primarily to prevent complete conversion. Table 1 indicates that the addition of HCl and H_2SO_4 had a negative effect on liquid hydrocarbon yield and conversion. We suspect that, although we did not test this hypothesis, the Cl and S poisoned the 10% Raney Ni catalyst and rendered the catalyst almost completely inactive.

Table 1 also summarizes the results of several active catalysts. The temporal variation of conversion and liquid hydrocarbon yield from these catalysts appear in Figure 8. Table 1 and Figure 8 reveal that the 10% Ni/ZrO_2 catalyst had a low liquid hydrocarbon yield and conversion, but a high selectivity to liquid products. The 10% Ni/Al_2O_3 catalyst showed the highest conversion, liquid hydrocarbon yield, and selectivity to liquid products. Last, the calcined Raney Ni catalyst had a high conversion, a relatively low liquid hydrocarbon yield, and a low selectivity to liquid products when compared to the 10% Ni/Al_2O_3 catalyst. Nonetheless, the calcined Raney Ni catalyst generally had higher liquid hydrocarbon yields than the 10%

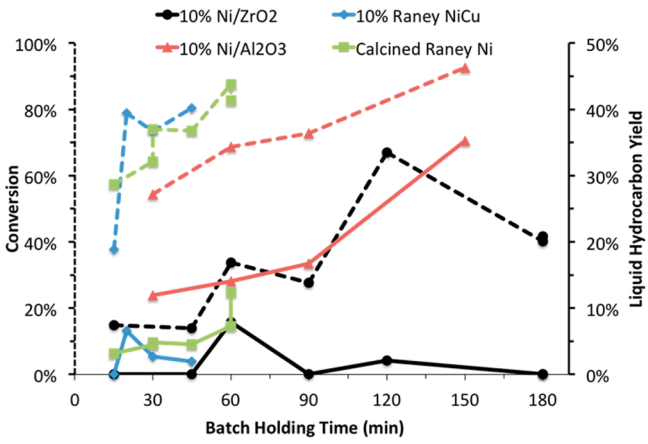

Figure 8. Conversion (dashed lines) and liquid hydrocarbon yield (solid lines) from Ni and NiCu catalysts in 4.1 mL batch reactors. Table 1 summarizes all of the catalysts tested. Conditions: 380 °C, 10 mg catalyst, 100 mg of *o*-cresol, 0.67 mL DI H_2O, 41 bar H_2 (STP), 6:1 H_2-to-*o*-cresol.

Raney NiCu catalyst. For the catalysts tested in Figure 8, the liquid hydrocarbons were cyclohexane, benzene, toluene, and methylcyclohexane. The major oxygenated products were methylcyclohexanol, methylcyclohexanone, phenol, cyclohexanol, and cyclohexanone. The gas product was primarily methane, with smaller amounts of CO_2. The yields of individual products are shown in SI Table S3.

The high liquid hydrocarbon yield from the 10% Ni/Al_2O_3 catalyst and the increased liquid hydrocarbon yield from the calcined Raney Ni catalyst support the hypotheses by Mortensen et al.[42] and Zhao et al.[32] that acid sites, such as those found in Al_2O_3, assist in C−O hydrogenolysis and, therefore, increase HDO activity. The results obtained with the calcined Raney Ni catalyst were especially encouraging because such a catalyst has not been studied previously for HDO. Furthermore, it is suspected that the liquid hydrocarbon yield, shown in Figure 8, was low because of the relatively high gasification activity of the catalyst (i.e., low selectivity to liquid products in Table 1), but in section 3.1, it was shown that Cu decreases the gasification activity of Raney Ni. Therefore, with these two tools, the addition of Cu and the addition of Al_2O_3, the activity and selectivity of Ni catalysts can be tuned.

3.2.2. Flow Reactions. At this point, this work identified several catalysts that are active for hydrothermal HDO, but several challenges remain. The first challenge is to obtain a high liquid hydrocarbon yield (e.g., > 50%) with these catalysts, and the second challenge is to determine the stability of these catalysts under the harsh hydrothermal conditions. These challenges were addressed by performing a series of flow reactor experiments using the reactor shown in Figure 1 and described in detail in the Methods section.

3.2.2.1. Calcined Raney Ni. Calcined Raney Ni was tested in the flow reactor, and Figure 9 shows the results. The conversion of *o*-cresol, at a W/F (mass of catalyst active metal/mass flow rate of *o*-cresol) of 12.7 min, is generally between 75 and 90% and appears to decrease slightly with TOS. The liquid hydrocarbon yield was generally between 25 and 45%, with the higher yields appearing at later TOS. The linear trend line fit to the liquid hydrocarbon yield data indicates an increasing liquid hydrocarbon yield with TOS. Figure 9 also shows that the yields of the two major liquid hydrocarbon products, methylcyclohexane and cyclohexane,

dx.doi.org/10.1021/cs500562u | ACS Catal. 2014, 4, 2605−2615

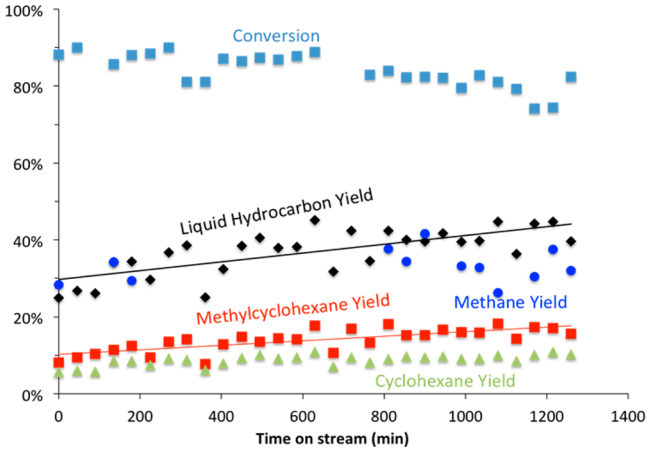

Figure 9. Results from reacting *o*-cresol over calcined Raney Ni. W/F = 12.7 min; T_{inlet} = 365 °C; T_{outlet} = 390 °C; 280 bar; feed flow rates (mL/min, ambient temperature): H_2O = 0.270, *o*-cresol = 0.030, internal standard solution = 0.400, H_2 = 0.006 mol/min; H_2-to-*o*-cresol molar ratio = 20:1, 550 °C in situ H_2 catalyst reduction.

appear relatively steady with TOS, if not increasing slightly. A variety of other minor liquid hydrocarbon products also formed and, in general, had low individual yields (<2%). The sum of these products, however, significantly increased the liquid hydrocarbon yield. These products include butane, 2-methylbutane, hexane, methylcyclopentane, 1,3-dimethylcyclopentane, ethylcyclopentane, toluene, and methylcyclohene (SI Table s4). These minor products indicate that this catalyst has a relatively high isomerization activity compared with the other catalysts examined.

Figure 9 shows that the methane yield was between 20 and 40% during the reaction, indicating that this catalyst still retains significant gasification activity. This gasification activity also appears to be maintained with TOS, indicating that this catalyst is unlikely to become more selective for liquid products, either oxygenated or hydrocarbons, without a modification to the catalyst.

Previous work revealed an increase in liquid hydrocarbon yield with TOS, similar to that in Figure 9, when using a Pt/C catalyst for the hydrothermal HDO of *o*-cresol. A potential cause of this increase in activity was reduction of the catalyst surface that had been oxidized during reactor startup.[21] Similarly, oxidation of the present Ni catalyst may have occurred during the reactor startup, and gradual rereduction during the reaction led to increasing liquid hydrocarbon yields. Another possible cause of the increase in liquid hydrocarbon yield with TOS is an increase in the Al_2O_3 content of the Raney Ni catalyst caused by the oxidizing hydrothermal environment. Suchanek developed an Al_2O_3–H_2O phase diagram by subjecting γ-$Al(OH)_3$ and γ-AlOOH to a hydrothermal environment and showed that under conditions similar to those used in this reaction, α-Al_2O_3 is formed.[44] Therefore, it is also possible that the increase in liquid hydrocarbon yield observed in Figure 9 is due to an increasing concentration of acid Al_2O_3 sites adjacent to the Ni active metal, allowing for HDO reactions to occur more readily.

Previous work with Raney Ni, using formic acid as the H_2 source and similar reaction conditions, provided only very low yields of liquid hydrocarbons, 6.4%, at a very similar W/F of 12 min.[21] Therefore, the development of calcined Raney Ni represents a significant step forward in developing a low-cost, active, and stable catalyst for hydrothermal HDO.

3.2.2.2. Supported NiCu catalyst. Figure 10 shows the results from reacting *o*-cresol over a 10%, 0.5% NiCu/Al_2O_3

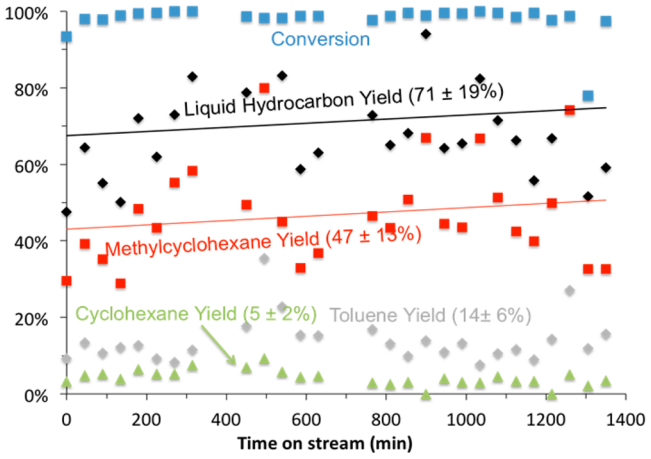

Figure 10. Results from reacting *o*-cresol over 10%, 0.5% NiCu/Al_2O_3. W/F = 3.22 min; T_{inlet} = 365 °C; T_{outlet} = 390 °C; 280 bar; feed flow rates (mL/min, ambient temperature): H_2O = 0.270, *o*-cresol = 0.030, internal standard solution = 0.400, H_2 = 0.006 mol/min; H_2 to *o*-cresol molar ratio = 20:1; 550 °C in situ H_2 catalyst reduction.

catalyst at a W/F of 3.22 min using the same reaction conditions as above. We doped this catalyst with a small amount of Cu (0.5%) to suppress the gasification pathway.

Figure 10 shows the conversion remained steady at ∼100% throughout the 24 h experiment. The liquid hydrocarbon yield was generally between 50 and 80%, with an average of 71 ± 19%. During this experiment, the reaction pressure would occasionally drop to around 225 bar, for an unknown reason, before rebuilding to 280 bar. These occasional process upsets induced atypical scatter in the data collected. Nonetheless, the results clearly show a high average liquid hydrocarbon yield and no significant catalyst deactivation over the 24 h reaction. The stability of this catalyst was surprising because of the reported instability of γ-Al_2O_3 under hydrothermal conditions.[8−10] It is worth noting that the two potential transformations of γ-Al_2O_3 under the reaction conditions used, γ-Al_2O_3 to AlOOH[9] or γ-Al_2O_3 to α-Al_2O_3,[44] would have occurred to a significant extent over the 24 h reaction, if either transformation was going to occur. The γ-Al_2O_3 may also have been stabilized by the presence of *o*-cresol or other alcohol-containing species in the reaction mixture.[45]

Figure 10 also shows that the yields of the three major liquid hydrocarbon products: cyclohexane, toluene, and methylcyclohexane. These three products accounted for >85% of the liquid hydrocarbon yield, but small yields of benzene (≤3%) and methylcyclohexene (≤2%) were also observed. This finding indicates that this supported catalyst is much less active for isomerization than the calcined Raney Ni catalyst.

The yields of oxygenated and gas products were generally low. The oxygenated products were phenol, cyclohexanone, cyclohexanol, 2-methylcyclohexanol, and 2-methylcyclohexanone, and the average yield for each oxygenated molecule was ≤2% (SI Table S5). The gas products were methane and CO_2, with average yields of 5 ± 2% and 3 ± 2%, respectively.

3.2.2.3. Calcined 5% Raney NiCu. The calcined Raney Ni catalyst tested in both batch and flow reactors showed very

dx.doi.org/10.1021/cs500562u | ACS Catal. 2014, 4, 2605−2615

promising results because of the increased liquid hydrocarbon yield when compared with previous work.[21] Examination of the products revealed that this catalyst was still too active for gasification because, as shown in Figure 9 and SI Table S4, between 20 and 40% of the carbon from *o*-cresol formed methane. Therefore, to suppress this gasification activity, we added 5% Cu to the calcined Raney Ni catalyst and reacted *o*-cresol over this catalyst at a *W*/*F* of 19.9 min.

Figure 11 shows that the *o*-cresol was completely converted over the calcined 5% Raney NiCu catalyst throughout the

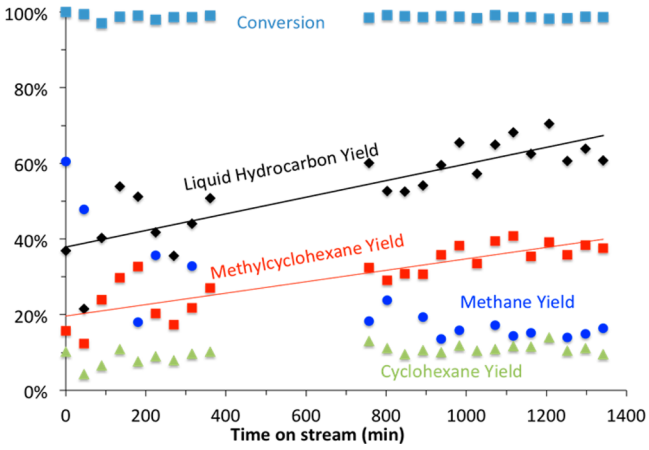

Figure 11. Results from reacting *o*-cresol over 5% calcined Raney NiCu. *W*/*F* = 19.9 min; T_{inlet} = 365 °C; T_{outlet} = 390 °C; 280 bar; feed flow rates (mL/min, ambient temperature): H_2O = 0.270, *o*-cresol = 0.030, internal standard solution = 0.400, H_2 = 0.006 mol/min; H_2 to *o*-cresol molar ratio = 20:1; 550 °C in situ H_2 catalyst reduction.

reaction. The liquid hydrocarbon yield was ∼40% early in the reaction and increased linearly to ∼60% after 1200 min on-stream. As with the calcined Raney Ni catalyst, the two major liquid hydrocarbon products were methylcyclohexane and cyclohexane. The methylcyclohexane yield increased linearly with TOS from ∼20 to ∼40%; the cyclohexane yield remained steady at 10 ± 2% over the course of the reaction. The remaining liquid hydrocarbon and oxygenated products (SI Table S6) were the same as those observed with the calcined Raney Ni catalyst, and each product had a low yield (≤2%).

Figure 11 also shows the methane yield from the calcined 5% Raney NiCu catalyst and indicates that at early TOS, the catalyst was active for gasification, but after 800 min on-stream, the gasification activity is lower and steady, producing methane in 17 ± 3% yield. This yield of methane compares favorably with the 34 ± 4% yield of methane observed with the calcined Raney Ni. Furthermore, this decrease in methane yield occurred even with an increase in *W*/*F* from 12.7 to 19.9 min. It is likely that this increase in selectivity toward liquid products and, more specifically, liquid hydrocarbon products, in the calcined 5% Raney NiCu catalyst is due primarily to the decrease in the gasification activity of the calcined 5% Raney NiCu catalyst compared with the calcined Raney Ni catalyst. The reason for the increase in the liquid hydrocarbon yield with TOS is again not known with certainty, but we speculate that this increase is due to the same reasons discussed above for the calcined Raney Ni catalyst.

All three catalysts tested in the flow reactor—calcined Raney Ni, $NiCu/Al_2O_3$, and calcined 5% Raney NiCu—represent significant advances in hydrothermal HDO catalysts because each catalyst produced moderate to high yields of liquid hydrocarbons while minimizing the production of gaseous products. Furthermore, each catalyst appeared to be free of any rapid deactivation, suggesting the catalyst lifetime is significantly longer than the 24 h time period tested. Last, these catalysts do not contain noble metals and do not require the addition of a separate acid catalyst (i.e., Nafion or H_3PO_4) to produce liquid hydrocarbons. Both of these factors have significant commercial implications because the catalyst is inexpensive and additional separation steps are not necessary to remove a homogeneous acid catalyst.

3.2.3. Catalyst Characterization. We performed XRD on the Ni/Al_2O_3, $NiCu/Al_2O_3$ and calcined Raney Ni catalysts. Figure 12 shows the XRD patterns of the γ-AlOOH; the

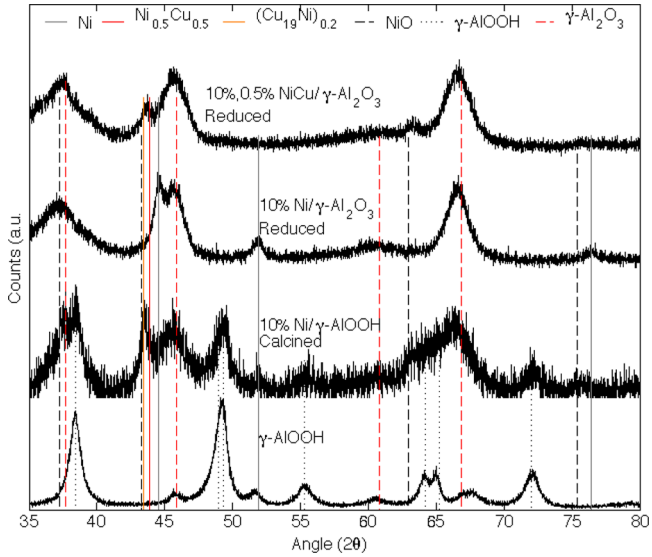

Figure 12. X-ray diffraction patterns of the γ-AlOOH; 10% Ni/Al_2O_3; and 10%, 0.5% $NiCu/Al_2O_3$ catalysts passivated in 1% O_2 at 70 °C overnight, Cu Kα source, 40 kV, 15 mA, 1.25°/min.

calcined 10% Ni/AlOOH; the reduced 10% Ni/Al_2O_3; and the reduced 10%, 0.5% $NiCu/Al_2O_3$ catalysts. The calcined Ni/AlOOH catalyst diffraction pattern contains NiO, AlOOH, and Al_2O_3 peaks, indicating that the AlOOH support is starting to convert to Al_2O_3. Reduction of the Ni/AlOOH catalyst converts the NiO to Ni and the remaining AlOOH to Al_2O_3. This outcome is evident by the absence of NiO and AlOOH peaks and the presence of Ni and Al_2O_3 peaks in the reduced Ni/Al_2O_3 pattern. In the 10%, 0.5% $NiCu/Al_2O_3$ catalyst diffraction pattern, only NiCu and Al_2O_3 phases appear. This result differs from the Raney NiCu catalysts in which both Ni and NiCu phases were observed. This result is likely because both the Ni and Cu were impregnated on the catalysts at the same time, whereas with the Raney NiCu catalysts, the Cu was added on top of the base Raney Ni catalyst.

Figure 13 shows the XRD patterns of the reduced Raney Ni, the calcined Raney Ni, and the calcined then reduced Raney Ni catalysts. The top two XRD patterns in Figure 13 zoom in on the baseline of the reduced Raney Ni and calcined/reduced Raney Ni patterns. The reduced Raney Ni pattern shows only Ni peaks, as expected. Upon calcination, much of the Ni in the original catalyst is converted to NiO, which is evident by the appearance of NiO peaks in this pattern. Upon initial inspection, reduction of the calcined Raney Ni catalyst returns

dx.doi.org/10.1021/cs500562u | ACS Catal. 2014, 4, 2605−2615

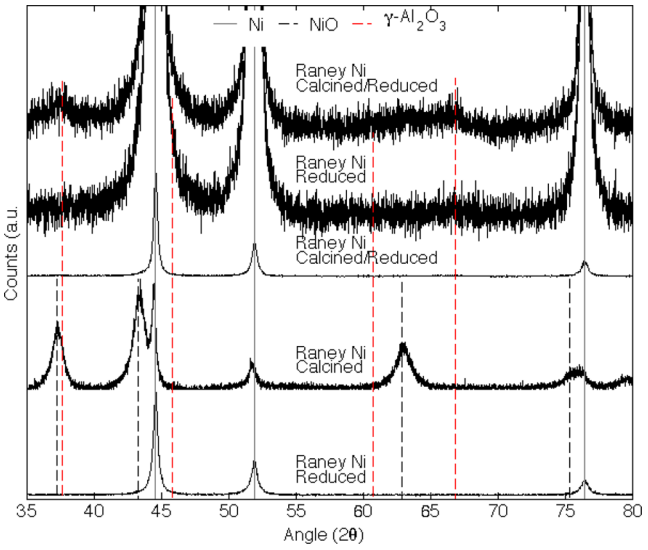

Figure 13. X-ray diffraction patterns of the Raney Ni catalysts passivated in 1% O_2 at 70 °C overnight, Cu Kα source, 40 kV, 15 mA, 1.25°/min.

the catalyst to an XRD pattern very similar to that of the reduced Raney Ni catalyst. The expanded patterns at the top of Figure 13, though, do indicate a slight difference between these catalysts. Upon careful inspection, one observes two new peaks at ∼37 and ∼67° in the calcined/reduced Raney Ni catalyst. These peak locations correspond to γ-Al_2O_3. This correspondence provides a strong indication that the calcination and reduction of the Raney Ni catalyst did result in the formation of Al_2O_3 and provides further supporting evidence that it is the presence of Al_2O_3 that increases the HDO activity of these catalysts. We also examined several expanded XRD patterns of the Raney NiCu catalysts shown in Figure 6 to be sure that the peaks seen in the expanded calcined/reduced Raney Ni catalyst pattern were not simply a shift in the baseline, and no evidence of the Al_2O_3 peaks was observed. Last, although not tested here, previous work with a Raney NiCu catalyst[21] indicated no change in the catalyst particle size between the fresh and used catalyst after a 24 h TOS reaction, thereby agreeing with the reaction results presented above.

4. CONCLUSION

This article demonstrates two approaches for improving the hydrothermal HDO activity and selectivity of Ni catalysts that, when combined, provide the only known stable and high liquid hydrocarbon yield for non-noble metal catalysts. The first approach is to dope the Ni catalysts with Cu to reduce the gasification activity. Between 7 and 25 wt % Cu added to the Raney Ni catalyst shifts the selectivity of the catalyst from gas to liquid products. Unfortunately, this shift in selectivity did not increase the liquid hydrocarbon yield. The second approach is to add acid sites because recent reports suggest that acid sites are important for the dehydration step in HDO.[31,42] Acid sites were added via an acidic support (Al_2O_3) for Ni and NiCu catalysts and via calcination of the Raney Ni catalyst to produce an Al_2O_3 phase within the catalyst. In flow reactor experiments, both the 10%, 0.5% NiCu/Al_2O_3 and the calcined 5% Raney NiCu catalysts produced liquid hydrocarbon yields over 60% and showed no activity loss over the 24 h reaction, indicating that these catalysts may have industrial relevance. In particular, the calcined 5% Raney NiCu catalyst represents an interesting hydrothermal HDO catalyst because of its novelty, activity, cost, and selectivity. Future research should focus on characterizing the metal surface of the fresh and used calcined Raney NiCu catalyst (e.g., temperature-programmed reduction, thermogravimetric analysis, X-ray photoelectron spectroscopy) and the acid sites (e.g., NH_3-TPD, pyridine infrared spectroscopy).

■ ASSOCIATED CONTENT

Ⓢ Supporting Information

Tables of product yields for all of the experiments performed. This material is available free of charge via the Internet at http://pubs.acs.org.

■ AUTHOR INFORMATION

Corresponding Author

*E-mail: psavage@umich.edu.

Notes

The authors declare no competing financial interest.

■ ACKNOWLEDGMENTS

We thank Thomas Yeh for performing the TEM/STEM imaging and Erin Branton for assisting with the reaction experiments. J. G. Dickinson acknowledges financial support from a NSF Graduate Research Fellowship. We gratefully acknowledge the National Science Foundation (Grant EFRI-0937992) and the College of Engineering for their financial support.

■ REFERENCES

(1) Furimsky, E. *Appl. Catal., A* **2000**, *124*, 470−477.
(2) Furimsky, E. *Catal. Today* **2013**, *217*, 13−56.
(3) Wang, H.; Male, J.; Wang, Y. *ACS Catal.* **2013**, *3*, 1047−1070.
(4) Bridgwater, A. V.; Meier, D.; Radlein, D. *Org. Geochem.* **1999**, *30*, 1479−1493.
(5) Yeh, T. M.; Dickinson, J. G.; Franck, A.; Linic, S.; Thompson, L. T.; Savage, P. E. *J. Chem. Technol. Biotechnol.* **2013**, *88*, 13−24.
(6) Valdez, P. J.; Dickinson, J. G.; Savage, P. E. *Energy Fuels* **2011**, *25*, 3235−3243.
(7) Brown, T. M.; Duan, P.; Savage, P. E. *Energy Fuels* **2010**, *24*, 3639−3646.
(8) Elliott, D. C.; Sealock, L. J., Jr; Baker, E. G. *Ind. Eng. Chem. Res.* **1993**, *32*, 1542−1548.
(9) Ravenelle, R. M.; Copeland, J. R.; Kim, W.-G.; Crittenden, J. C.; Sievers, C. *ACS Catal.* **2011**, *1*, 552−561.
(10) Yu, J.; Savage, P. E. *Appl. Catal., B* **2001**, *31*, 123−132.
(11) Furimsky, D. E. *Ind. Eng. Chem. Res.* **2013**, *52*, 17695−17713.
(12) Bond, J. Q.; Alonso, D. M.; Wang, D.; West, R. M.; Dumesic, J. A. *Science* **2010**, *327*, 1110−1114.
(13) Braden, D. J.; Henao, C. A.; Heltzel, J.; Maravelias, C. C.; Dumesic, J. A. *Green Chem.* **2011**, *13*, 1755−1765.
(14) Davda, R. R.; Shabaker, J. W.; Huber, G. W.; Cortright, R. D.; Dumesic, J. A. *Appl. Catal., B* **2003**, *43*, 13−26.
(15) Huber, G. W.; Cortright, R. D.; Dumesic, J. A. *Angew. Chem. Int. Ed* **2004**, *43*, 1549−1551.
(16) Kunkes, E. L.; Simonetti, D. A.; West, R. M.; Serrano-Ruiz, J. C.; Gärtner, C. A.; Dumesic, J. A. *Science* **2008**, *322*, 417.
(17) Zhao, C.; Kou, Y.; Lemonidou, A. A.; Li, X.; Lercher, J. A. *Angew. Chem.* **2009**, *121*, 4047−4050.
(18) Zhao, C.; He, J.; Lemonidou, A. A.; Li, X.; Lercher, J. A. *J. Catal.* **2011**, *280*, 8−16.
(19) Zhao, C.; Lercher, J. A. *ChemCatChem* **2012**, *4*, 64−68.
(20) Zhao, C.; Camaioni, D. M.; Lercher, J. A. *J. Catal.* **2012**, *288*, 92−103.

(21) Dickinson, J. G.; Savage, P. E. *J. Mol. Catal. A: Chem.* **2014**, *388*−*389*, 56−65.
(22) Dickinson, J. G.; Poberezny, J. T.; Savage, P. E. *Appl. Catal., B* **2012**, *123*−*124*, 357−366.
(23) Duan, P.; Savage, P. E. *Appl. Catal., B* **2011**, *108*−*109*, 54−60.
(24) Duan, P.; Savage, P. E. *Appl. Catal., B* **2011**, *104*, 136−143.
(25) Duan, P.; Savage, P. E. *Energy Environ. Sci.* **2011**, *4*, 1447−1456.
(26) Duan, P.; Savage, P. E. *Ind. Eng. Chem. Res.* **2011**, *50*, 52−61.
(27) Duan, P.; Savage, P. E. *Bioresour. Technol.* **2011**, *102*, 1899−1906.
(28) Fu, J.; Shi, F.; Thompson, L. T., Jr; Lu, X.; Savage, P. E. *ACS Catal.* **2011**, *1*, 227−231.
(29) Fu, J.; Lu, X.; Savage, P. E. *Energy Environ. Sci.* **2010**, *3*, 311−317.
(30) Fu, J.; Lu, X.; Savage, P. E. *ChemSusChem* **2011**, *4*, 481−486.
(31) Zhao, C.; Kou, Y.; Lemonidou, A. A.; Li, X.; Lercher, J. A. *Chem. Commun.* **2010**, *46*, 412−414.
(32) Zhao, C.; Kasakov, S.; He, J.; Lercher, J. A. *J. Catal.* **2012**, *296*, 12−23.
(33) Zhao, C.; Lercher, J. A. *Angew. Chem.* **2012**, *124*, 6037−6042.
(34) Sitthisa, S.; Pham, T.; Prasomsri, T.; Sooknoi, T.; Mallinson, R. G.; Resasco, D. E. *J. Catal.* **2011**, *280*, 17−27.
(35) Mullen, C. A.; Boateng, A. A.; Goldberg, N. M.; Lima, I. M.; Laird, D. A.; Hicks, K. B. *Biomass Bioenerg.* **2010**, *34*, 67−74.
(36) Ross, A. B.; Biller, P.; Kubacki, M. L.; Li, H.; Lea-Langton, A.; Jones, J. M. *Fuel* **2010**, *89*, 2234−2243.
(37) Choe, S. J.; Kang, H. J.; Kim, S.; Park, S.; Park, D. H.; Huh, D. S. *Bull. Korean Chem. Soc.* **2005**, *26*, 1682.
(38) Andersson, M. P.; Abild-Pedersen, F.; Remediakis, I. N.; Bligaard, T.; Jones, G.; Engbæk, J.; Lytken, O.; Horch, S.; Nielsen, J. H.; Sehested, J. *J. Catal.* **2008**, *255*, 6−19.
(39) Huber, G. W.; Shabaker, J. W.; Dumesic, J. A. *Science* **2003**, *300*, 2075.
(40) Shabaker, J. W.; Huber, G. W.; Dumesic, J. A. *J. Catal.* **2004**, *222*, 180−191.
(41) Shabaker, J. W.; Simonetti, D. A.; Cortright, R. D.; Dumesic, J. A. *J. Catal.* **2005**, *231*, 67−76.
(42) Mortensen, P. M.; Grunwaldt, J. D.; Jensen, P. A.; Jensen, A. D. *ACS Catal.* **2013**, *3*, 1774−1785.
(43) Cheng, W. C.; Czarnecki, L. J.; Pereira, C. J. *Ind. Eng. Chem. Res.* **1989**, *28*, 1764−1767.
(44) Suchanek, W. L. *J. Am. Ceram. Soc.* **2010**, *93*, 399−412.
(45) Ravenelle, R. M.; Copeland, J. R.; Pelt, A. H.; Crittenden, J. C.; Sievers, C. *Top. Catal.* **2012**, *55*, 162−174.